

Formation mechanism of the (2 × 1) reconstruction of calcite (104)

Haojun Zhou¹, Yingquan Chen¹, Mingyue Ding² and Xiaoliang Zhong^{1,*}

¹School of Energy and Power Engineering, Huazhong University of Science and Technology, Wuhan 430074, China

²School of Power and Mechanical Engineering, Wuhan University, Wuhan 430072, China.

e-mail: xzhong@hust.edu.cn

Abstract

Calcite has recently attracted extensive research interest in fields ranging from geoscience to carbon dioxide removal. Although much effort has been made to study the (2x1) reconstruction of the most stable (104) surface, the origin of this reconstruction remains unclear. Here, we carefully investigate the atomic and electronic structures of calcite (104) via density functional theory methods with van der Waals corrections. The results unambiguously show that the driving force for this reconstruction is the intrinsic demands of surface atoms to increase the coordination numbers. On reconstructing, calcite (104) forms four additional Ca-O bonds per (2x1) unit cell. Besides, phonon spectrums indicate both unreconstructed and reconstructed surfaces are dynamically stable. Finally, by applying the climbing image nudged elastic band method, an energy barrier is predicted during the reconstructing. This work delivers a full picture for the formation of calcite (104)-(2x1) reconstruction and can greatly advance the understanding of surface science for calcite.

Calcium carbonate (CaCO_3) is one common substance on Earth. It is the major constituent of limestone, marble, eggshells, and pearls. As the major polymorph of CaCO_3 in nature¹, calcite has been actively investigated in fields including geoscience^{2, 3, 4}, soil stabilization^{5, 6}, carbon dioxide removal⁷, and new material development^{8, 9}. The most stable face of calcite is the (104) surface with the fewest Ca–O bonds broken upon surface formation¹⁰. This surface supports virtually all processes involving calcite¹¹. It is known that surface reconstruction can have a profound impact on crystal growth, surface properties and application of crystalline materials^{12, 13, 14}. Since 1990s, a range of surface sensitive analysis techniques including low-energy electron diffraction (LEED)¹⁵, X-ray photoelectron spectroscopy (XPS)^{15, 16}, grazing incidence X-ray diffraction (GIXRD)¹⁷ and atomic force microscopy (AFM)^{11, 18, 19, 20, 21} have been applied to detect the (2x1) reconstruction of calcite (104). On the other hand, theoretical studies including molecular dynamics (MD) simulations^{10, 22, 23} and density functional theory (DFT) calculations^{11, 21, 24} have been performed to search for the atomic model of this reconstructed surface and to provide insight into the origin of the (2x1) reconstruction. Recently, by combining high-resolution non-contact atomic force microscopy (NC-AFM) data and DFT calculations, it is established that the (2x1) reconstruction is thermodynamically the most stable form of calcite (104)¹¹.

Regarding the origin of the calcite (104)-(2x1) reconstruction, the early views proposed in the 1990s include cation ordering^{25, 26}. This viewpoint was recently rebutted by Rohl et al. via DFT calculations¹¹. In 2003 Rohl et al. used MD methods and pointed out that an imaginary phonon mode of the unreconstructed surface signifying the necessity of surface reconstruction²². Nevertheless, vibrational properties obtained by MD simulations should be treated with caution since these simulations use empirical potentials²⁷ and it is known that in some cases MD methods don't yield satisfactory results for calcite²⁸. Calculations based on more accurate quantum mechanical methods are thus highly desired to check this. Stipp et al. also performed MD simulations and proposed that step edges may be responsible for the (2x1) reconstruction¹⁰. However, the step edge effect becomes negligible for terrace sizes larger than 4.5 nm¹⁰ and subsequent AFM studies where cleaved surfaces were shown to be flat reported the reconstruction^{11, 19}. Very recently, Rahe et al. stated that the origin of the (2x1) reconstruction was 'purely thermodynamic' via DFT simulations¹¹. Yet it remains unclear why the reconstructed surface has a lower total energy. Besides, it is not known whether the (2x1) reconstructing is a spontaneous process, or an energy barrier exists during the reconstructing, i.e., the nature of reconstruction.

In the present work, we make efforts towards obtaining a fundamental understanding of the calcite (104)-(2x1) reconstruction by applying DFT methods. We note that DFT simulations have recently played an important role in elucidating the mechanisms of crystal surface reconstruction^{29, 30, 31, 32} due to the relatively high accuracy and capability of investigating the underlying electronic structure in depth. Our results unambiguously show that the (2x1) reconstruction is resulted from the intrinsic demands of surface atoms to increase the coordination numbers. We have also calculated vibrational properties to check if the unreconstructed surface has imaginary phonon modes. Finally, the climbing image nudged elastic band (CI-NEB) method³³ is applied to ascertain if there is an energy barrier during the reconstructing.

Results and discussion

Structure characteristics of reconstructed calcite (104)

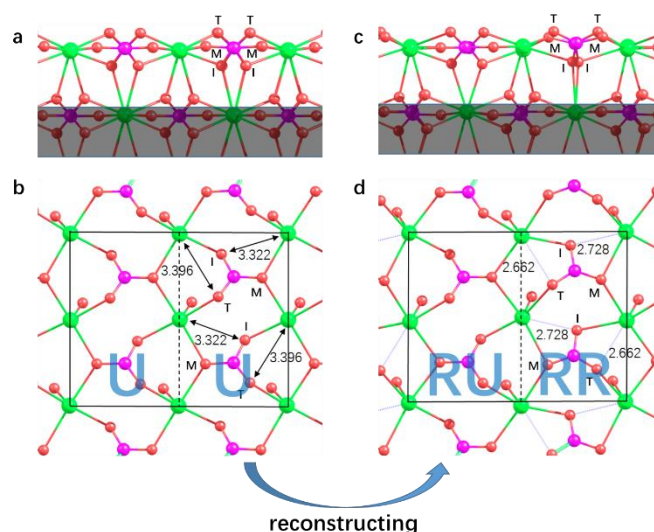


Fig. 1 | Atomic structures of unreconstructed and reconstructed calcite (104). Top and bottom panels are side view and top view, respectively. The shaded area of the side view is not shown in the top view for clarity. The unreconstructed surface (U) is shown on the left while the reconstructed one is shown on the right. RU and RR represent the unreconstructed half and the reconstructed half of a (2x1) unit cell of the reconstructed surface, respectively. Colour scheme: Ca in green, C in purple, and O in red. T = topmost, M = middle, I = innermost.

We first describe the structural features of both unreconstructed and reconstructed calcite (104) surfaces. The optimized calcite bulk lattice constants are $a = b = 5.027 \text{ \AA}$, and $c = 17.061 \text{ \AA}$, compared well with the experimental values³⁴ (4.991 and 17.062 \AA). In calcite bulk, each Ca atom is bonded to six O atoms while each O atom binds with two Ca atoms. All Ca-O bond lengths (nearest Ca-O distance) are 2.368 \AA . The next-nearest (NN) Ca-O distance is considerably greater (3.481 \AA). In the top layer of the unreconstructed surface, coordination number (CN) of each Ca atom is reduced to five (Fig. 1a, b). Each outmost O atom of one carbonate group binds with only one Ca atom while the other two O atoms still bind with two Ca atoms. The (2x1) reconstruction features a rotation of the carbonate group within one half (called ‘the reconstructed half’, denoted by ‘RR’ hereafter) of each (2x1) unit cell while structure variation in the other half (called ‘the unreconstructed half’, denoted by ‘RU’) is much less apparent^{11, 22} (Fig. 1c,d). Atomic structure of the optimized reconstructed (104) surface is essentially the same as that obtained by Rahe¹¹ since both simulations are at the same level of theory. It is to be noted that based on this structure, NC-AFM images at different tip-sample distances have been successively reproduced¹¹. Previously, a similar reconstructed structure obtained by MD simulations was shown to be able to reproduce the experimental LEED pattern²².

We identify that upon surface reconstructing, each surface CO_3^{2-} group in RR forms two *additional* Ca-O bonds. As Fig.1 shows, each topmost O atom (T) in RR moves towards one NN Ca atom. Rotation of the CO_3^{2-} group of about 18° renders a significant decrease in the corresponding Ca-O distance from 3.396 \AA (Fig. 1b) to 2.662 \AA (Fig. 1d), i.e., a reduction of about 0.7 \AA . Likewise, distance between each innermost O atom (I) and one NN Ca atom substantially decreases from

3.322 Å to 2.728 Å (reduction ≈ 0.6 Å). The two Ca-O bonds (2.662 and 2.728 Å) formed upon reconstruction are about 0.3 Å longer than the nearest Ca-O distance in the bulk (2.368 Å) and are about 0.8 Å shorter than the NN Ca-O distance (3.481 Å). One may raise a question why previous studies haven't discussed these two additional bonds (as far as the authors are aware). One reason may be that these chemical bonds are relatively longer such that some graphical programs don't show the bonding, therefore the drastic changes in Ca-O distances were overlooked. On the other hand, all five nearest Ca-O distances associated with one CO_3^{2-} group within the right half of the (2x1) cell in Fig. 1b increase upon reconstructing, but the magnitude of variation is relatively small (no greater than 0.11 Å). In the left half of the (2x1) cell in Fig. 1b, three out of the five nearest Ca-O distances associated with one CO_3^{2-} group increase upon reconstructing, with maximum change being ~ 0.05 Å. The other two nearest Ca-O distances decrease slightly (change no greater than ~ 0.01 Å).

Electronic structure analyses on calcite (104)

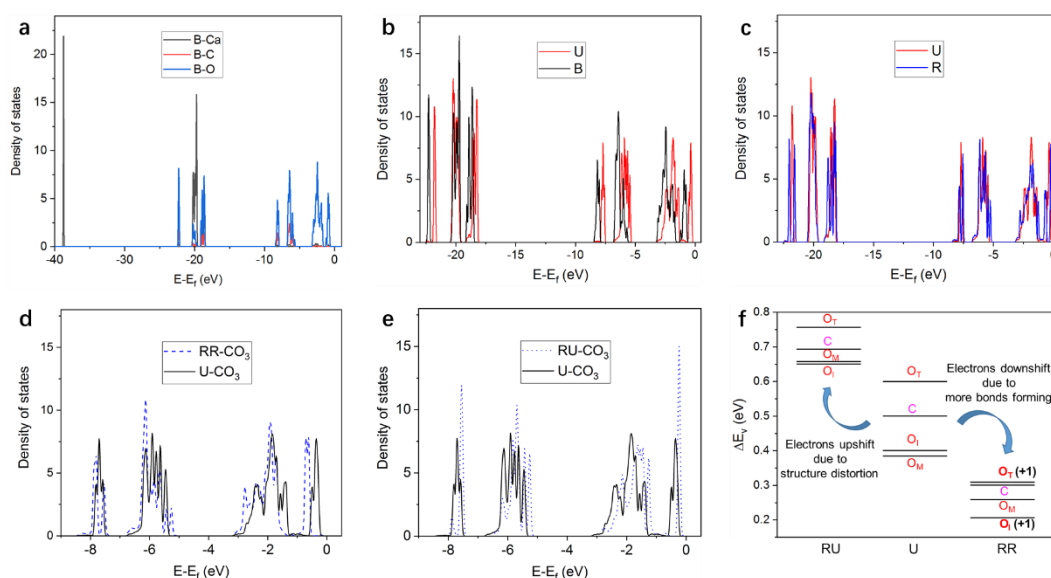


Fig. 2 | Calcite electronic structures: bulk, unreconstructed and reconstructed (104). **a** DOS of calcite bulk (B) projected on different species. **b** DOS of bulk and unreconstructed (U) (104). **c** DOS of unreconstructed and reconstructed (R) (104). **d** DOS associated with one carbonate group in RR (RR- CO_3) versus in the unreconstructed surface (U- CO_3). **e** DOS associated with one carbonate group in RU (RU- CO_3) versus in the unreconstructed surface. **f** Shift of valence electron levels associated with one carbonate group in U, RU and RR. O_T , O_I and O_M stand for the topmost, innermost and middle oxygen atoms, respectively (see Fig. 1). '+1' in the brackets means coordination number increases by 1.

We now discuss calcite electronic structures which underlie the energetics. Fig 2.a shows the density of states (DOS) of calcite bulk. In line with literature³⁵, Ca shows high peaks around -38 and -20 eV, respectively. DOS is dominated by C and O electrons in the energy range close to Fermi level (-10 to 0 eV). Moreover, O has much higher DOS than C does, as a result of the 3:1 atomic ratio and the stronger ability to attract electrons. Atomic charge is estimated by Bader analysis. In calcite bulk, atomic charge of Ca, C and O is +1.63, +2.17 and -1.27, respectively. Due to the reduced coordination numbers, energies of surface atoms are higher than those of the bulk counterparts. Accordingly, DOS spectrum of the unreconstructed surface in general shifts to the right compared

with that of the bulk (Fig 2.b). For clarity surface DOS peak around -38 eV is not shown in Fig 2.b, which only differs from the corresponding bulk peak slightly. On the other hand, change in atomic charge is small at the surface, with maximum variation smaller than 0.02 for all three species. DOS of the surface is taken to be that associated with atoms in the top layer. We show in Supplementary Fig. 1 that DOS of inner layers only differs from that of bulk slightly. Fig 2.c compares DOS spectrums of unreconstructed and reconstructed surfaces. One notes that DOS peaks of the reconstructed surface are typically lower and broader, reflecting the lower symmetry of the reconstructed structure. Nevertheless, DOS spectrums of both surfaces in general overlap with each other, underlying the nearly degenerate surface energies^{11, 24}.

We show in Fig. 1 that on reconstructing, the surface forms four additional bonds per (2x1) unit cell. We now discuss the impact of these ‘newly formed’ bonds on electronic structures. Fig. 2 d shows that DOS spectrum associated with each CO_3^{2-} group in RR shifts to the lower energy range compared with that in U. DOS below -9 eV is not shown for clarity, which also shifts to the lower energy range. This means CO_3^{2-} groups in RR are thermodynamically more stable than those in U. In contrast, DOS spectrum of each CO_3^{2-} group in RU shifts to the higher energy range (Fig.2 e). To better analyze the shift in DOS, we calculate the (average) valence electron energy level E_{v-x} of an atom x by Eq. (1)

$$E_{v-x} = \frac{\int_{-\infty}^{E_f} E_x D(E_x) dE_x}{\int_{-\infty}^{E_f} D(E_x) dE_x} \quad (1)$$

where E_x is valence electron energy of atom x and $D(E_x)$ is the corresponding DOS. We then define valence electron level shift (ΔE_{v-x}) to be the difference between E_{v-x} of a surface atom and that of its bulk counterpart as given by Eq. (2)

$$\Delta E_{v-x} = E_{v-x}(\text{surface}) - E_{v-x}(\text{bulk}) \quad (2)$$

As Fig. 2f shows, at the unreconstructed surface the topmost oxygen atoms (O_T) have the highest ΔE_v as a result of CN reduction (from two to one). Upon reconstructing, in RR each outmost oxygen atom (O_T) and each innermost oxygen atom (O_I) forms one additional bonds with Ca (Fig. 1). O_T and O_I in RR exhibit noticeable lowering in valence electron energy, with change in ΔE_v being -0.29 and -0.19 eV, respectively (Fig. 2f). As a result, the difference between $\Delta E_{v-\text{O}_T}$ and $\Delta E_{v-\text{C}}$ is much smaller in RR than in U. Regarding O_I , in RR $\Delta E_{v-\text{O}_I}$ becomes lower than $\Delta E_{v-\text{O}_M}$ while in U the contrary is true. For C and O_M , although CNs don't change on reconstructing, hybridization between carbon and oxygen states within each CO_3^{2-} group (Fig 2.a) renders a downshift of the corresponding electronic states in RR (Fig. 2f). On the other hand, Ca-O bond lengths in RU mainly increase (as discussed above). Accordingly, electron energies associated with C and O in RU increase (Fig. 2e,f).

We have also looked into surface Ca atoms, each of which forms two additional bonds with oxygen on reconstructing. $\Delta E_{v-\text{Ca}}$ of the reconstructed surface is 0.15 eV lower than that of the unreconstructed surface. The less significant variation in Ca electron energy may be related to the lower lying of Ca electron states (Fig. 2a), which are therefore less sensitive to chemical environment change. In summary, electron energies of all C and O atoms decrease in RR, as a result of CN increase and hybridization between oxygen and carbon states. Ca electrons also shift down due to CN increase although the change is relatively small. On the contrary, electron energies of all C and O atoms shift up in RU caused by the elongation of Ca-O bonds. Therefore, coordination

number increase is the key in stabilizing the reconstructed surface, which decrease electron energies of surface Ca atoms and electron energies of C/O atoms in RR.

Dynamic stability of calcite (104)

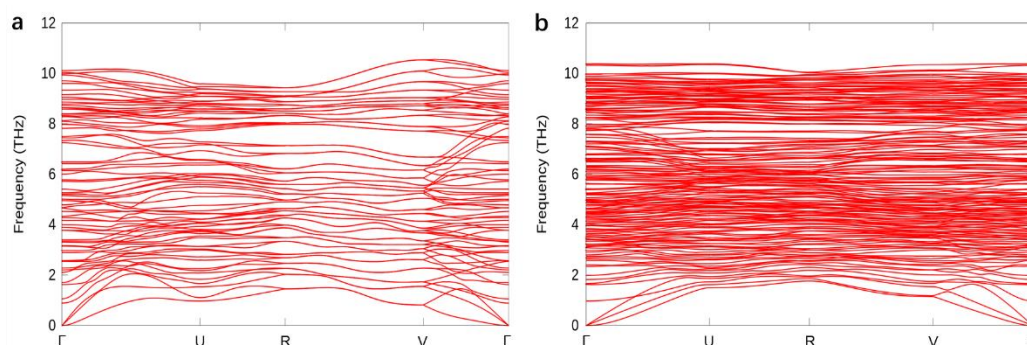


Fig. 3 | Vibrational properties of calcite (104). **a** Phonon spectrum of the unreconstructed surface. **b** Phonon spectrum of the reconstructed surface. Special points in the two-dimensional Brillouin zone: $\Gamma(0,0)$, $U(0.5,0)$, $R(0.5,0.5)$ and $V(0, 0.5)$.

By performing MD simulations Rohl et al. showed there was an imaginary phonon mode for the unreconstructed surface and suggested that the (2x1) reconstruction was a spontaneous process²². However, in a more recent study Magdans et al. reported the unreconstructed (104) surface under both dry and humid atmospheric conditions with GIXRD¹⁷. This signals the stability of the unreconstructed surface and therefore one would expect an energy barrier separating the unreconstructed and the reconstructed states. To address this problem, we have calculated phonon spectrums for both unreconstructed and reconstructed (104) as shown in Fig. 3. It is apparent that there are more bands in the phonon spectrum of the reconstructed surface, as a result of the symmetry reduction. Rohl reported that the imaginary phonon mode of the unreconstructed surface located at (0.5,0) in the Brillouin zone²², which is the U point in Fig. 3. However, our DFT simulations show that although U is a local minimum of the lowest phonon band for the unreconstructed surface, the corresponding frequency is positive (~0.9 THz). In both panels of Fig. 3 no imaginary phonon mode exists. Consequently, our study presents a picture that both the unreconstructed and reconstructed surfaces are dynamically stable. We have also calculated phonon spectrum of the unreconstructed surface applying PBE functional and the DFT-D3 method with Becke-Johnson damping^{36,37} (illustrated in Supplementary Fig. 3). The results show that there is no imaginary phonon mode associated with the unreconstructed surface, irrespective the method applied within the DFT framework. Therefore, our DFT results supports Magdans's work which reported the unreconstructed (104) surface under both dry and humid conditions¹⁷.

Probing the possible energy barrier during reconstructing

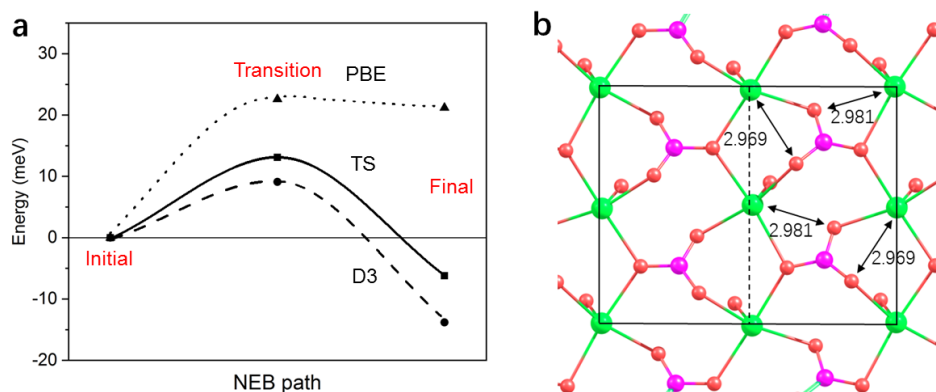


Fig. 4 | Probing the possible energy barrier during calcite (104) reconstructing. **a** Minimum energy path calculated by the CI-NEB method. ‘Initial’, ‘Transition’ and ‘Final’ represent the initial state (unreconstructed surface), the transition state, and the final state (reconstructed surface), respectively. **b** Atomic structure of TS.

We have also applied the CI-NEB method³³ to probe the possible energy barrier. As Fig. 4a shows, there appears to be a single energy barrier between the two states. Fig. 4b shows that in the transition state carbonate groups rotate about 10° in the right half of the (2x1) unit cell, compared with 18° in the final reconstructed state. The two Ca-O distances corresponding to the two ‘newly formed’ Ca-O bonds when fully reconstructed are 2.969 and 2.981 Å, respectively. These values are about 0.6 Å greater than the nearest Ca-O distance in bulk (2.368 Å) and are about 0.5 Å smaller than the NN Ca-O distance (3.481 Å). Therefore, the transition state can be understood as a state where these two additional Ca-O bonds are about to be formed. The activation energy (E_a) is 14 meV per (2x1) unit cell for the formation of the reconstructed surface. Conversely, E_a for the transition from a reconstructed surface to an unreconstructed one is 20 meV per unit cell. Considering that the calculated activation energy is rather small, we have also applied the PEB functional and the DFT-D3 method with Becke-Johnson damping^{36, 37} to check this. In line with literature^{11, 24}, while both DFT methods with van der Waals interactions predict that the reconstructed surface is slightly favored, the semilocal PEB functional predicts that the unreconstructed one is favored. Nevertheless, Fig. 4a shows that there is a non-vanishing but low energy barrier between the unreconstructed and the reconstructed surface, irrespective of the DFT method used.

In summary, by applying DFT methods with van der Waals corrections, we unambiguously show that the calcite (104)-(2x1) reconstruction is driven by the demands of surface atoms to increase the coordination numbers. At the surface four additional Ca-O bonds are formed per (2x1) unit cell on reconstructing as a result of carbonate group rotation. Within the surface layer, electron energies associated with carbonate groups in RR and Ca atoms are effectively lowered due to new bonds forming. In contrast to Rohl’s work²² which performed MD simulations, our DFT phonon spectrums indicate both the unreconstructed and the reconstructed surfaces are stable. The low energy barrier obtained by CI-NEB method suggests that the detected surface structure should be critically dependent on the experimental conditions. Very recently, it has been shown that calcite (2x1) reconstruction can have a decisive impact on calcite adsorption properties^{11, 21, 38}. We believe our

findings can significantly advance the understanding of surface-related phenomena of calcite.

Methods

DFT calculations

All calculations are performed via the Vienna ab-initio simulation package (VASP)³⁹ Projector-augmented wave (PAW) potentials⁴⁰ with the Tkatchenko–Scheffler method with iterative Hirshfeld partitioning⁴¹. Plane-wave cutoff energy is set to 500 eV and the convergence of energy is 10^{-6} eV. $5 \times 8 \times 5$ and $2 \times 3 \times 1$ Monkhorst–Pack k-point meshes are set to calculate calcite bulk and (104), respectively. Atomic and electronic structure analyses are based on 7-layer fully-optimized structures, although we have found a 4-layer model is thick enough to obtain the converged surface energy (in line with Rahe’s work¹¹). Phonon analyses and CI-NEB calculations are performed via the 4-layer model (including 12 atomic layers). Phonon spectrums are calculated using the finite difference approach. In NEB calculations we include four images between the initial state and the final state to start the simulations. We have also tested including six images, with the results essentially the same.

References

1. Morse JW, Arvidson RS, Lüttge A. Calcium Carbonate Formation and Dissolution. *Chemical Reviews* **107**, 342-381 (2007).
2. Amidon WH, Kylander-Clark ARC, Barr MN, Graf SFI, West DP. Pace of passive margin tectonism revealed by U-Pb dating of fracture-filling calcite. *Nature Communications* **13**, 1953 (2022).
3. Daëron M, *et al.* Most Earth-surface calcites precipitate out of isotopic equilibrium. *Nature Communications* **10**, 429 (2019).
4. Laanait N, Callagon EBR, Zhang Z, Sturchio NC, Lee SS, Fenter P. X-ray-driven reaction front dynamics at calcite-water interfaces. *Science* **349**, 1330-1334 (2015).
5. Feng K, Montoya BM. Influence of Confinement and Cementation Level on the Behavior of Microbial-Induced Calcite Precipitated Sands under Monotonic Drained Loading. *Journal of Geotechnical and Geoenvironmental Engineering* **142**, (2016).
6. Montoya BM, DeJong JT. Stress-Strain Behavior of Sands Cemented by Microbially Induced Calcite Precipitation. *Journal of Geotechnical and Geoenvironmental Engineering* **141**, (2015).
7. Pogge von Strandmann PAE, *et al.* Rapid CO₂ mineralisation into calcite at the CarbFix storage site quantified using calcium isotopes. *Nature Communications* **10**, 1983 (2019).
8. Natalio F, *et al.* Flexible Minerals: Self-Assembled Calcite Spicules with Extreme Bending Strength. *Science* **339**, 1298-1302 (2013).
9. Li H, Xin HL, Muller DA, Estroff LA. Visualizing the 3D Internal Structure of Calcite Single Crystals Grown in Agarose Hydrogels. *Science* **326**, 1244-1247 (2009).
10. Kristensen R, Stipp SLS, Refson K. Modeling steps and kinks on the surface of calcite. *The Journal of Chemical Physics* **121**, 8511-8523 (2004).
11. Heggemann J, Ranawat YS, Krejčí O, Foster AS, Rahe P. Differences in Molecular Adsorption Emanating from the (2 × 1) Reconstruction of Calcite(104). *The Journal of Physical Chemistry Letters* **14**, 1983-1989 (2023).
12. Srivastava GP. Theory of semiconductor surface reconstruction. *Reports on Progress in Physics* **60**, 561 (1997).
13. Ohtake A. Surface reconstructions on GaAs(001). *Surface Science Reports* **63**, 295-327 (2008).

14. Gao L, Cui X, Sewell CD, Li J, Lin Z. Recent advances in activating surface reconstruction for the high-efficiency oxygen evolution reaction. *Chemical Society Reviews* **50**, 8428-8469 (2021).
15. Stipp SL, Hochella MF. Structure and bonding environments at the calcite surface as observed with X-ray photoelectron spectroscopy (XPS) and low energy electron diffraction (LEED). *Geochimica et Cosmochimica Acta* **55**, 1723-1736 (1991).
16. Stipp SLS. Toward a conceptual model of the calcite surface: hydration, hydrolysis, and surface potential. *Geochimica et Cosmochimica Acta* **63**, 3121-3131 (1999).
17. Magdams U, Gies H, Torrelles X, Rius J. Investigation of the {104} surface of calcite under dry and humid atmospheric conditions with grazing incidence X-ray diffraction (GIXRD). *European Journal of Mineralogy* **18**, 83-91 (2006).
18. Stipp SLS, Eggleston CM, Nielsen BS. Calcite surface structure observed at microtopographic and molecular scales with atomic force microscopy (AFM). *Geochimica et Cosmochimica Acta* **58**, 3023-3033 (1994).
19. Schütte J, *et al.* Clear Signature of the (2 × 1) Reconstruction of Calcite (101 $\bar{4}$). *Langmuir* **26**, 8295-8300 (2010).
20. Rahe P, Schütte J, Kühnle A. NC-AFM contrast formation on the calcite (10N14) surface. *Journal of Physics: Condensed Matter* **24**, 084006 (2012).
21. Heggemann J, *et al.* Water adsorption lifts the (2 × 1) reconstruction of calcite(104). *Physical Chemistry Chemical Physics*, (2023).
22. Rohl AL, Wright K, Gale JD. Evidence from surface phonons for the (2 × 1) reconstruction of the (101 $\bar{4}$) surface of calcite from computer simulation. *American Mineralogist* **88**, 921-925 (2003).
23. Tao L, Li Z, Wang G-C, Cui B-Y, Yin X-T, Wang Q. Evolution of calcite surface reconstruction and interface adsorption of calcite-CO₂ with temperature. *Materials Research Express* **6**, 025035 (2019).
24. Akiyama T, Nakamura K, Ito T. Atomic and electronic structures of CaCO₃ surfaces. *Physical Review B* **84**, 085428 (2011).
25. Wenk HR, Meisheng H, Lindsey T, Morris JW. Superstructures in ankerite and calcite. *Physics and Chemistry of Minerals* **17**, 527-539 (1991).
26. Reksten K. Superstructures in calcite. *American Mineralogist* **75**, 807-812 (1990).

27. Akinwande D, *et al.* A review on mechanics and mechanical properties of 2D materials—Graphene and beyond. *Extreme Mechanics Letters* **13**, 42-77 (2017).
28. Ukita M, Toyoura K, Nakamura A, Matsunaga K. Pressure-induced phase transition of calcite and aragonite: A first principles study. *Journal of Applied Physics* **120**, (2016).
29. Li G, *et al.* Role of Antiferromagnetic Ordering in the (1×2) Surface Reconstruction of Ca(Fe_{1-x}Cox)₂As₂. *Physical Review Letters* **112**, 077205 (2014).
30. Hu L, Huang B, Liu F. Atomistic Mechanism Underlying the Si(111)-(7×7) Surface Reconstruction Revealed by Artificial Neural-network Potential. *Physical Review Letters* **126**, 176101 (2021).
31. Shen Y, Morozov SI, Luo K, An Q, Goddard lii WA. Deciphering the Atomistic Mechanism of Si(111)-7 × 7 Surface Reconstruction Using a Machine-Learning Force Field. *Journal of the American Chemical Society* **145**, 20511-20520 (2023).
32. Yuan W, *et al.* Direct in-situ insights into the asymmetric surface reconstruction of rutile TiO₂ (110). *Nature Communications* **15**, 1616 (2024).
33. Sheppard D, Xiao P, Chemelewski W, Johnson DD, Henkelman G. A generalized solid-state nudged elastic band method. *The Journal of Chemical Physics* **136**, 074103 (2012).
34. Maslen EN, Streltsov VA, Streltsova N. X-ray study of the electron density in calcite, CaCO₃. *Acta Crystallographica Section B-structural Science* **49**, 636-641 (1993).
35. Hossain FM, Murch GE, Belova IV, Turner BD. Electronic, optical and bonding properties of CaCO₃ calcite. *Solid State Communications* **149**, 1201-1203 (2009).
36. Grimme S, Antony J, Ehrlich S, Krieg H. A consistent and accurate ab initio parametrization of density functional dispersion correction (DFT-D) for the 94 elements H-Pu. *The Journal of Chemical Physics* **132**, (2010).
37. Grimme S, Ehrlich S, Goerigk L. Effect of the damping function in dispersion corrected density functional theory. *Journal of Computational Chemistry* **32**, 1456-1465 (2011).
38. Dickbreder T, Lautner D, Köhler A, Klausfering L, Bechstein R, Kühnle A. How water desorbs from calcite. *Physical Chemistry Chemical Physics* **25**, 12694-12701 (2023).
39. Kresse G, Hafner J. Ab initio molecular dynamics for liquid metals. *Physical Review B* **47**, 558-561 (1993).
40. Kresse G, Joubert DP. From ultrasoft pseudopotentials to the projector augmented-wave method. *Physical Review B* **59**, 1758-1775 (1999).

41. Bučko T, Lebègue S, Hafner J, Ángyán JG. Improved Density Dependent Correction for the Description of London Dispersion Forces. *Journal of Chemical Theory and Computation* **9**, 4293-4299 (2013).